arXiv:1406.7095v4 [nucl-th] 22 Jun 2015

First application of Fayans functional to deformed nuclei

S V Tolokonnikov[1,2], I N Borzov[1,3], M Kortelainen[4,5], Yu S Lutostansky[1], and E E Saperstein[1,6]

[1]Kurchatov Institute, 123182 Moscow, Russia
[2] Moscow Institute of Physics and Technology, Dolgoprudny, Russia
[3] Joint Institute for Nuclear Research, 141980 Dubna, Russia
[3] Department of Physics, P.O. Box 35 (YFL), University of Jyväskylä, FI-40014 Jyväskylä, Finland
[4] Helsinki Institute of Physics, P.O. Box 64, FI-00014 University of Helsinki, Finland
[6] National Research Nuclear University MEPhI, 115409 Moscow, Russia

E-mail: tolkn@mail.ru, ibor48@mail.ru, markus.kortelinen@jyu.fi, lutostansky@yandex.ru, saper43_7@mail.ru

Abstract. First calculations for deformed nuclei with the Fayans functional are carried out for the uranium and lead isotopic chains. The ground state deformations and deformation energies are compared to Skyrme-Hartree-Fock-Bogolyubov HFB-17 and HFB-27 functional results. For the uranium isotopic chain, the Fayans functional property predictions are rather similar to HFB-17 and HFB-27 predictions. However, there is a disagreement for the lead isotopic chain. Both of the Skyrme HFB functionals lead to predictions of rather strong deformations for the light Pb isotopes, which does not agree with the experimental data on charge radii and magnetic moments of the odd Pb isotopes. On the other hand, the Fayans functional leads to the prediction of a spherical ground state for all of the lead isotopes, in accordance with the data and the results known from the literature obtained with the Gogny D1S force and the SLy6 functional as well. The deformation energy curves are calculated and compared against those derived from four Skyrme functionals—SLy4, Sly6, SkM* and UNEDF1—for the ^{238}U nucleus and several lead-deficient Pb isotopes. In the first case, the Fayans functional result is rather close to SkM* and UNEDF1 ones, which—in particularly the latter—describe the first and second barriers in ^{238}U rather well. For the light lead isotopes, the Fayans deformation energy curves are qualitatively close to those derived from the SLy6 functional.

1. Introduction

A long-standing goal of the low-energy nuclear theory community is to have a unified theoretical framework, applicable to nuclear structure and reactions. Presently, due to computational limitations, *ab initio* approaches are applicable to light or medium mass closed-shell nuclei only. Therefore, microscopical theories which use effective forces with phenomenological parameters are usually applied to describe the entire nuclear chart. Nuclear density functional theory (DFT) provides the most popular such models. In the framework of nuclear DFT, complex many-body correlations are encoded into the energy density functional (EDF), constructed from the nuclear densities and currents. Historically, since the work by Vautherin and Brink [1], the Hartree-Fock (HF) method with the effective Skyrme forces has become very popular in nuclear physics. From the very beginning, the Skyrme HF method was aimed at calculating global properties of nuclei, such as the binding energy and neutron and proton density distributions. A little later the HF method with the effective Gogny force was suggested [2] and successfully applied to the same objects as the Skyrme HF method had been applied too. In addition to these approaches, relativistic mean-field (RMF) model methods have also been employed in nuclear physics; see [3] and references therein. In fact, it was quite soon realized that these methods had a rather strong correspondence with DFT methods employed e.g. in atomic physics. Indeed, during the last few decades, mean-field methods in the framework of HF and Hartree-Fock-Bogolyubov (HFB) theory have been widely used in nuclear physics [4, 5]. The HFB, a method suitable for superfluid nuclei with pairing correlations, is a generalization of the HF approach, which allows particles and holes to be treated on an equal footing.

The use of density-dependent effective interactions is a common feature of these mean-field approaches. When Skyrme and Gogny effective forces are written as a form of EDF, a rather simple ansatz for density dependence is assumed. Schematically it reads

$$E_0^{\rm int}[\rho] = \int \mathcal{E}(\rho(\mathbf{r}))d^3r = \int \frac{a\rho^2}{2}\left(1+\alpha\rho^\sigma\right)d^3r, \tag{1}$$

where $\rho(\mathbf{r})$ is the matter density and a, α, and $\sigma \leq 1$ are parameters. For brevity, we omit for a time the isotopic indices and do not discuss the spin-orbit and other "small" terms of the effective force. As will be discussed later, Fayans functional has more sophisticated density dependence [6, 7, 8, 9, 10]. Recently, the density dependence of Skyrme-like EDFs has been enriched by utilizing density matrix expansion techniques [11, 12, 13, 14, 15, 16].

The parameters of Skyrme forces, as well as Gogny and RMF models, have been typically adjusted to the experimental data on nuclear binding energies and charge radii. Many optimization schemes also use data on single-particle levels and fission properties, together with other observables and pseudo-observables. Because data on nuclei that are very neutron rich are scarce, and were especially scarce at the time when some of the older Skyrme parameterizations were adjusted, some of the isovector parameters

may have larger uncertainties. The best description of nuclear masses (the root-mean-square deviation from the respective experimental values being smaller than 600 keV) was attained with the HFB-17 EDF by the Brussels-Montreal Collaboration [17, 18]. This result was achieved, however, by including some phenomenological corrections on top of the mean field.

The Fayans functional [6, 7, 8, 9, 10] used in this work assumes a rather sophisticated density dependence which can be schematically written as

$$\mathcal{E}(\rho) = \frac{a\rho^2}{2}\frac{1+\alpha\rho^\sigma}{1+\gamma\rho^\sigma}, \tag{2}$$

where γ is one of the EDF parameters. The use of the bare mass, i.e. $m^* = m$, is another peculiarity of the Fayans functional. Both of these features of the Fayans approach are connected to the self-consistent theory of finite Fermi systems (TFFS) [19].

Up to now, all applications of the Fayans functional were limited to spherical nuclei. In addition to the aforementioned investigations, they included the analysis of charge radii [20], of the magnetic [21, 22] and quadrupole [23, 24] moments in odd nuclei, of characteristics of the first 2^+ excitations in even semi-magic nuclei [25, 26] and of beta-decay [27] as well. Recently, single-particle spectra of magic nuclei have been analyzed [28]. In all of the aforementioned cases, a reasonable description of the data was achieved—better as a rule than that achieved in analogous Skyrme HFB calculations.

It is worth discussing briefly another new recently developed approach, initially known as the Barcelona-Catania-Paris EDF and latterly as the Barcelona-Catania-Paris-Madrid (BCPM) EDF. The volume part of the BCPM EDF is found from the infinite nuclear matter Brueckner–Hartree–Fock approach, by using a realistic free NN potential. The infinite nuclear matter equation of the state (EOS) is then approximated within a good accuracy by two polynomials: one for the isoscalar and one for the isovector components. In addition to this, the EDF contains a finite range term and a term for the spin-orbit force. This approach was initially formulated in [29], whereas the final form of the corresponding EDF was developed in [30]. Later, the properties of the BCPM EDF have been developed and investigated further [31, 32, 33, 34, 35, 36, 37]. In [35], masses of 579 nuclei were fitted with the rms deviation of 1.58 MeV. The charge radii were also described with a very good accuracy. To some extent, the BCPM EDF is similar to the Fayans EDF. Indeed, the volume part of the FaNDF^0 functional, used in the present work, was adjusted [9] to the Friedman and Pandharipande nuclear and neutron matter EOS [38]. Similarly, the volume part of the BCPM, given by Baldo *et. al.* [29, 30], was also adjusted to the calculated nuclear matter EOS. The use of a bare mass, that is $m^* = m$, is another common feature of these two EDFs.

The aim of this work is to apply, for the first time, the Fayans functional in the study of deformed nuclei. The principle goal is to study deformation properties of Fayans functional for a selected set of isotopic chains. This will pave the way for more comprehensive studies with the Fayans functional across the nuclear chart. In the present work, the general finite range structure of the Fayans EDF [6, 7, 8] is localized to a form which is closer to the Skyrme EDFs. This allows us to employ the computer code

HFBTHO [39], developed for Skyrme EDFs, with some modifications. This article is organized as follows. In section 2, the path from the self-consistent TFFS to the Fayans functional is outlined. In section 3, the version FaNDF^0 [9] of the Fayans functional is briefly described. Section 4 presents the results for U and Pb isotopes calculated with the set [9] of FaNDF^0 parameters. Section 5 contains our conclusions.

2. Self-consistent TFFS and the Fayans functional

The self-consistent TFFS [19] is based on the general principles of TFFS [40] supplemented with the condition of self-consistency in the TFFS among the energy-dependent mass operator $\Sigma(\mathbf{r_1}, \mathbf{r_2}; \varepsilon)$, the single-particle Green's function $G(\mathbf{r_1}, \mathbf{r_2}; \varepsilon)$, and the effective NN interaction $\mathcal{U}(\mathbf{r_1}, \mathbf{r_2}, \mathbf{r_3}, \mathbf{r_4}; \varepsilon, \varepsilon')$ [41].

This approach starts from the quasiparticle mass operator $\Sigma_q(\mathbf{r_1}, \mathbf{r_2}; \varepsilon)$ which, by definition [40], coincides with the exact mass operator Σ at the Fermi surface. In the mixed coordinate-momentum representation the operator $\Sigma_q(\mathbf{r}, k^2; \varepsilon)$ depends linearly on the momentum squared k^2 and the energy ε [40, 19],

$$\Sigma_q(\mathbf{r}, k^2; \varepsilon) = \Sigma_0(\mathbf{r}) + \frac{1}{2m\varepsilon_{\rm F}^0}\,\mathbf{k}\,\Sigma_1(\mathbf{r})\mathbf{k} + \Sigma_2(\mathbf{r})\frac{\varepsilon}{\varepsilon_{\rm F}^0}, \tag{3}$$

where $\varepsilon_{\rm F}^0 = (k_{\rm F}^0)^2/2m$ is the Fermi energy of nuclear matter, $k_{\rm F}^0$ being the corresponding Fermi momentum. By definition, we have

$$\Sigma_0(\mathbf{r}) = \Sigma(\mathbf{r}, k^2; \varepsilon)\big|_0\,, \tag{4}$$

$$\Sigma_1(\mathbf{r}) = \varepsilon_{\rm F}^0\,\frac{\partial\Sigma(\mathbf{r}, k^2; \varepsilon)}{\partial\varepsilon_k}\bigg|_0\,, \tag{5}$$

$$\Sigma_2(\mathbf{r}) = \varepsilon_{\rm F}^0\,\frac{\partial\Sigma(\mathbf{r}, k^2; \varepsilon)}{\partial\varepsilon}\bigg|_0\,, \tag{6}$$

where $\varepsilon_k = k^2/2m$ and the subscribe '0' means that the energy and momentum variables are taken at the Fermi surface. Thus, the component Σ_2 determines the Z-factor:

$$Z(\mathbf{r}) = \left(1 - \Sigma_2(\mathbf{r})/\varepsilon_{\rm F}^0\right)^{-1}, \tag{7}$$

whereas the inverse effective mass is

$$\frac{m}{m^*(\mathbf{r})} = \frac{(1 + \Sigma_1(\mathbf{r})/\varepsilon_{\rm F}^0)}{(1 - \Sigma_2(\mathbf{r})/\varepsilon_{\rm F}^0)}. \tag{8}$$

Usually, the quantity inverse to the numerator is called the 'k-mass', and the denominator, the 'E-mass'.

The wave functions $\psi_\lambda(\mathbf{r})$ which diagonalize the quasiparticle Green function $G_q = (\varepsilon - \varepsilon_k - \Sigma_q)^{-1}$ obey the following equation:

$$\left(\Sigma_0(\mathbf{r}) - \frac{1}{2m\varepsilon_{\rm F}^0}\nabla\Sigma_1(\mathbf{r})\nabla + \Sigma_2(\mathbf{r})\frac{\varepsilon_\lambda}{\varepsilon_{\rm F}^0}\right)\psi_\lambda = \varepsilon_\lambda\psi_\lambda. \tag{9}$$

They are orthonormalized with the weight,

$$\int d\mathbf{r}\,\psi_\lambda^*(\mathbf{r})\,\psi_{\lambda'}(\mathbf{r})\,\left(1 - \Sigma_2(\mathbf{r})/\varepsilon_{\rm F}^0\right) = \delta_{\lambda\lambda'}. \tag{10}$$

The Lagrange formalism was used in Ref. [19], with the quasiparticle Lagrangian L_q being constructed in such a way that the corresponding Lagrange equations coincide with equation (9).

In the doubly magic nuclei, which are non-superfluid, the Lagrangian density $\mathcal{L}_q$, with $L_q = \int d\mathbf{r}\mathcal{L}_q(\mathbf{r})$, depends on three sorts of densities $\nu_i(\mathbf{r}),\ i = 0, 1, 2$:

$$\nu_0(\mathbf{r}) = \sum n_\lambda \psi^*_\lambda(\mathbf{r})\psi_\lambda(\mathbf{r}), \tag{11}$$

$$\nu_1(\mathbf{r}) = -\frac{1}{2m\varepsilon^0_{\rm F}} \sum n_\lambda \nabla\psi^*_\lambda(\mathbf{r})\nabla\psi_\lambda(\mathbf{r}), \tag{12}$$

$$\nu_2(\mathbf{r}) = \frac{1}{\varepsilon^0_{\rm F}} \sum n_\lambda \varepsilon_\lambda \psi^*_\lambda(\mathbf{r})\psi_\lambda(\mathbf{r}), \tag{13}$$

where ε_λ and n_λ are the quasiparticle energies and occupation numbers, and $n_\lambda = (0, 1)$. Evidently, one gets

$$\nu_0(\mathbf{r}) = Z(\mathbf{r})\rho(\mathbf{r}), \tag{14}$$

where the density $\rho(\mathbf{r})$ is normalized to the total particle number. The relation between $\nu_1(\mathbf{r})$ and the Skyrme density $\tau(\mathbf{r})$ is more complicated [19]. The density $\nu_2(\mathbf{r})$ has no analogue in the Skyrme HF theory.

The components Σ_i of the mass operator (3) can be found from the interaction Lagrangian $L'_q[\nu_i]$ as follows:

$$\Sigma_i = \frac{\delta L'_q}{\delta\nu_i}. \tag{15}$$

The simplest ansatz for the quasiparticle Lagrangian which involves the momentum and energy dependence effects on an equal footing was suggested in [19]:

$$\mathcal{L}'_q = -C_0\left(\frac{1}{2}\nu_0\hat{\lambda}_{00}\nu_0 + \frac{\gamma}{6\rho_0}\nu_0^3 + \hat{\lambda}_{01}\nu_0\nu_1 + \hat{\lambda}_{02}\nu_0\nu_2\right), \tag{16}$$

where $C_0 = (dn/d\varepsilon_{\rm F})^{-1} = \pi^2/(p_{\rm F}m)$ is the usual TFFS normalization factor, the inverse density of states at the Fermi surface, and $\rho_0 = (k^0_{\rm F})^3/3\pi^2$ is the density of one kind of nucleon in equilibrium symmetric nuclear matter. The amplitudes

$$\hat{\lambda}_{ik} = \lambda_{ik} + \lambda'_{ik}\tau_1\tau_2 \tag{17}$$

are the isotopic matrices and only one of them,

$$\hat{\lambda}_{00}(\mathbf{r}_1, \mathbf{r}_2) = \hat{\lambda}_{00}(1 + r_0^2\triangle_1)\delta(\mathbf{r}_1, \mathbf{r}_2), \tag{18}$$

is the finite range operator. The term proportional to γ in equation (16) results in the density dependence of the main, scalar and isoscalar, Landau–Migdal interaction amplitudes [40].

To minimize the number of new parameters, the ansatz $\lambda'_{01} = \lambda'_{02} = 0$ was used in [19]. In this case, the components Σ^τ_1 and Σ^τ_2 of the mass operator do not depend on τ, being functions of the total density $\nu^+_0 = \nu^n_0 + \nu^p_0$:

$$\Sigma^\tau_1(\mathbf{r}) = \frac{\delta L_q}{\delta\nu^\tau_2(\mathbf{r})} = C_0\lambda_{01}\nu^+_0(\mathbf{r}), \tag{19}$$

$$\Sigma_2^\tau(\mathbf{r}) = \frac{\delta L_q}{\delta \nu_2^\tau(\mathbf{r})} = C_0 \lambda_{02} \nu_0^+(\mathbf{r}). \tag{20}$$

With the use of (14) and (20), one can obtain the explicit dependence of the Z-factor on the density with the usual normalization:

$$Z_\tau(\mathbf{r}) = \frac{2}{1 + \sqrt{1 - 4C_0\lambda_{02}\rho^+(\mathbf{r})/\varepsilon_{\mathrm{F}}^0}}. \tag{21}$$

The total interaction energy can be found for the Lagrangian (16) according the canonical rules. It corresponds to the following EDF:

$$\mathcal{E}_{\mathrm{int}} = C_0 \left[\frac{1}{2}\hat{\lambda}_{00} \left(\nu_0^2 - r_p^2 (\nabla \nu_0)^2 \right) + \hat{\lambda}_{01} \nu_0 \nu_1 + \frac{\gamma}{6\rho_0} \nu_0^3 \right]. \tag{22}$$

It does not contain the 'new' density ν_2 and converts to the Skyrme EDF at the limit where $\nu_0 \to \rho$ and $\nu_1 \to \tau$. However, the replacement of equation (14) with the Z-factor (21) results in a rather sophisticated EDF in the self-consistent TFFS, which can hardly be introduced *ad hoc*.

The parameters of the Lagrangian (16) were found in [19] by fitting binding energies, charge radii and single-particle spectra of doubly magic nuclei from ^{40}Ca to ^{208}Pb. The obtained values of $\lambda_{01} = 0.31$ and $\lambda_{02} = -0.25$ correspond to the following characteristics of nuclear matter: $m_0^* = 0.95m$ and $Z_0 = 0.8$. The latter agrees with the value found in [42] on the base of the dispersion relation for the quantity $\partial\Sigma/\partial\varepsilon$ [40] in nuclear matter.

In [6], the so-called generalized EDF method was formulated as a generalization of the Kohn–Sham (KS) method [43] for superfluid nuclei. In this case, the EDF depends not only on the normal densities $\rho_{\mathrm{n,p}}(\mathbf{r})$, but on their anomalous counterparts $\nu_{\mathrm{n,p}}(\mathbf{r})$ as well. Independently, similar development of the KS method was suggested in condensed matter physics [44]. The pairing problem was considered in [6], with an elegant method of direct solving Gor'kov equations for spherical systems in the coordinate representation [45]. In practice, this method is close to that of solving HFB equations which was presented first in [2] for the Gogny EDF and in [46] for the Skyrme EDF.

The KS method is based on the Hohenberg–Kohn theorem [47], stating that the ground state energy of a Fermi system is a functional of its density. Unfortunately, this theorem does not give any recipe to construct the EDF. Fayans *et al.* [6] found that the EDF (22) can be rather accurately approximated with a rational ρ-dependence of equation (2) type. In addition, they used the ansatz $m^* = m$ typical for the KS method. This also agrees well with the above estimation. Thus, the Fayans functional can be interpreted as a simplified version of the self-consistent TFFS [19], and the 'denominator' in the EDF (2) appears due to the energy dependence effects taken into account in the TFFS.

It is worth mentioning that the use of any EDF with density dependence leads to serious problems if one tries to go beyond mean-field multi-reference calculations, such as particle number projection or angular momentum projection [48, 49, 50, 51]. Therefore, in this work, we use Fayans functional for single-reference calculations only.

Three sets of the EDF parameters, DF1–DF3, were suggested in Ref. [8], but the most part of calculations with Fayans EDF were carried out with the set DF3 [10] or

its version DF3a for transuranium region [52]. Although up to now there have been no systematic calculations of nuclear binding energies across the whole nuclear chart within this method, isotopic chains of spherical nuclei were examined in [10, 20, 52]. It was found that the accuracy is only a little less good than that of the best Skyrme HFB calculations. As for the accuracy of reproducing the charge radii [20] of spherical nuclei, typical deviation is of the order of 0.01–0.02 fm, i.e. the agreement is on a par with or better than that from Skyrme EDF models. This may be linked to more adequate density dependence of the Fayans EDF as compared to the Skyrme one. Indeed, if we denote the average error in describing the binding energies as $\overline{\delta E}$ and that for the charge radii as $\overline{\delta R_{\rm ch}}$, these quantities should be, due to the Hohenberg–Kohn theorem [47], proportional to each other:

$$\overline{\delta R_{\rm ch}} = \alpha\, \overline{\delta E}\,, \tag{23}$$

where the coefficient α depends on the functional that we use. Often, a fine tuning of the EDF parameters is performing by focusing mainly on reproduction of the nuclear masses within a minimal value of $\overline{\delta E}$. In this case, the accuracy of reproducing the charge radii is proportional to the coefficient α. As the analysis of [20] showed, for the Fayans EDF this coefficient is less than those of the HFB-17 and SLy4 functionals. Again, this observation may linked to more enriched density dependence of Fayans functional, which allows to incorporate complex many-body correlations more efficiently. The Fayans EDF also provides a high quality description of magnetic [21, 22] and quadrupole [23, 24] moments of odd spherical nuclei, energies and $B(E2)$ values for even semi-magic nuclei [25, 26]. Recent analysis [28] of the single-particle energies of doubly magic nuclei obtained with the Fayans functional versus the HFB-17 one also provides evidence in favor of the former.

Up to now, all self-consistent calculations with Fayans functionals were carried out for spherical nuclei only. In [52], deformations of the transuranium nuclei were taken into account approximately. This work presents the first application of the Fayans functional in studying axially deformed nuclei.

3. FaNDF^0 functional

For completeness, we write down explicitly main ingredients of the Fayans EDF method. In this method, the ground state energy of a nucleus is considered as a functional of normal and anomalous densities,

$$E_0 = \int \mathcal{E}[\rho(\mathbf{r}), \nu(\mathbf{r})] d^3r, \tag{24}$$

where the isotopic indices and the spin-orbit densities are for brevity omitted.

The main distinctions between this method and the Skyrme EDF approach lie in the normal part of the EDF $\mathcal{E}_{\rm norm}$, containing the central and spin-orbit terms, and the Coulomb interaction term for protons. In most applications of this method [7, 8, 10], the DF3 functional was used with the finite range Yukawa-type central force. In this

work we use the EDF FaNDF^0 from [9] with a localized form of the Yukawa function, $\mathrm{Yu}(r) \to 1 - r_c^2\nabla^2$, which makes the structure of the surface part of the EDF closer to that from the Skyrme functionals. This form allows us to use a modified version of the computer code HFBTHO [39], originally constructed for Skyrme-like EDFs. The parameters of FaNDF^0 were fitted to the EOS of nuclear and neutron matter by Friedman and Pandharipande [38] and the masses of lead and tin isotopes.

The volume part of the EDF, $\mathcal{E}^{\mathrm{v}}(\rho)$, is taken as a fractional function of densities $\rho_+ = \rho_n + \rho_p$ and $\rho_- = \rho_n - \rho_p$:

$$\mathcal{E}^{\mathrm{v}}(\rho) = C_0 \left[a_+^{\mathrm{v}} \frac{\rho_+^2}{4} f_+^{\mathrm{v}}(x) + a_-^{\mathrm{v}} \frac{\rho_-^2}{4} f_-^{\mathrm{v}}(x) \right], \tag{25}$$

where

$$f_+^{\mathrm{v}}(x) = \frac{1 - h_{1+}^{\mathrm{v}} x^\sigma}{1 + h_{2+}^{\mathrm{v}} x^\sigma} \tag{26}$$

and

$$f_-^{\mathrm{v}}(x) = \frac{1 - h_{1-}^{\mathrm{v}} x}{1 + h_{2-}^{\mathrm{v}} x}. \tag{27}$$

Here, $x = \rho_+/\rho_0$ is the dimensionless nuclear density. The power parameter $\sigma = 1/3$ is chosen in the FaNDF^0 functional, in contrast to the case for DF3, where $\sigma = 1$ is used. The structure of other terms in the volume parts of these two functionals is kept the same. However, the above difference leads to significantly different values of the dimensionless parameters in equations (25)–(27) although they still correspond to the same characteristics of nuclear matter, the incompressibility $K_0 = 220$ MeV, equilibrium density $\rho_0 = 0.160$ fm^{-3} ($r_0 = 1.143$ fm), and energy per particle $\mu = -16.0$ MeV. The parameters denoted by '+' are $a_+^{\mathrm{v}} = -9.559$, $h_{1+}^{\mathrm{v}} = 0.633$, $h_{2+}^{\mathrm{v}} = 0.131$, and the parameters denoted by '-' are $a_-^{\mathrm{v}} = 4.428$, $h_{1-}^{\mathrm{v}} = 0.25$, $h_{2-}^{\mathrm{v}} = 1.300$, which all are dimensionless quantities. This parameter set corresponds to the asymmetry energy coefficient of $a_{\mathrm{sym}} = 30.0$ MeV.

In [53], a set of criteria were suggested for the Skyrme EDFs. For the nuclear matter part these criteria were connected to properties of the saturation point and to the second derivatives of the energy density $\mathcal{E}^{\mathrm{v}}(\rho_+, \rho_-)$. Using the notations of [53], the so-called skewness coefficient of the symmetrical nuclear matter is equal to

$$Q_0 = 27\rho_0^3 \left(\frac{\partial^3 \mathcal{E}(\rho_+, \rho_-)/\rho_+}{\partial \rho_+^3} \right)_{x=1, y=0}, \tag{28}$$

where $y = \rho_-/\rho_0$ is a dimensionless neutron excess. To simplify the expressions for the mixed higher density derivatives, we introduce a nuclear matter energy function

$$S(\rho_+) = \frac{1}{2}\rho_+^2 \left(\frac{\partial^2 \mathcal{E}(\rho_+, \rho_-)/\rho_+}{\partial \rho_-^2} \right)_{y=0}. \tag{29}$$

The first and second density derivatives of this function are

$$L_0 = 3\rho_0 \left(\frac{\partial \mathcal{S}(\rho_+)}{\partial \rho_+} \right)_{x=1}, \tag{30}$$

Table 1. Nuclear matter characteristics for differen EDFs, all of which are given in MeV except the matter density ρ_0.

EDF	ρ_0, fm^{-3}	μ	$a_{\rm sym}$	K_0	Q_0	L_0	$K_{\rm sym}$
FaNDF^0	0.160	-16.00	30.00	220.00	-427.14	29.96	- 149.22
SkM*	0.160	-15.77	30.03	216.61	-386.09	45.78	- 155.94
SLy4	0.160	-15.97	32.00	229.91	-363.11	45.94	-119.73
SLy6	0.159	-15.92	31.96	229.86	-360.24	47.45	-112.71

and

$$K_{\rm sym} = 9\rho_0^2 \left(\frac{\partial^2 \mathcal{S}(\rho_+)^2}{\partial \rho_+} \right)_{x=1}. \tag{31}$$

The numerical values of the above quantities for the FaNDF^0 functional are presented in table 1 where they are compared to the Skyrme EDFs taken from [53], which are used in the present work. One can see that the differences between all of the listed main nuclear matter characteristics are usually small.

The main difference between FaNDF^0 and DF3 functionals lies in the structure of the surface term. Now it is as follows:

$$\mathcal{E}^{\rm s}(\rho) = C_0 \frac{1}{4} \frac{a_+^{\rm s} r_0^2 (\nabla \rho_+)^2}{1 + h_+^{\rm s} x^\sigma + h_\nabla^{\rm s} r_0^2 (\nabla x_+)^2}, \tag{32}$$

with $h_+^{\rm s} = h_{2+}^{\rm v}$, $a_+^{\rm s} = 0.600$, $h_\nabla^{\rm s} = 0.440$.

The usual form for the direct Coulomb term of the EDF of [9] is employed; the folded charge density $\rho_{\rm ch}$ is found taking into account the proton and neutron form factors. As regards the exchange Coulomb term, it was taken as follows:

$$-\frac{3}{4}\left(\frac{3}{\pi}\right)^{1/3} e^2 \rho_{\rm p}^{4/3} (1 - h_{\rm Coul} x_+^\sigma), \tag{33}$$

with $h_{\rm Coul} = 0.941$. Such a strong suppression, in comparison with the Slater approximation with $h_{\rm Coul} = 0$, helps with solving the so-called Nollen–Schiffer anomaly [54]. It is worth mentioning that a similar suppression of the Coulomb exchange term was adopted in some Skyrme functionals [55].

The usual form for the TFFS spin-orbit term [40] was used in FaNDF^0 with the same spin-orbit parameters as in the DF3 functional [10]. Note that the FaNDF^0 functional does not contain the effective tensor, in contrast to the DF3 [7] and DF3a [52] EDFs.

For completeness, we write out explicitly the anomalous term of the EDF [9]:

$$\mathcal{E}_{\rm anom} = C_0 \sum_{i=n,p} \nu_i^\dagger(\mathbf{r}) f^\xi(x_+(\mathbf{r})) \nu_i(\mathbf{r}), \tag{34}$$

where the density-dependent dimensionless effective pairing force is

$$f^\xi(x_+) = f_{\rm ex}^\xi + h^\xi x_+ + f_\nabla^\xi r_0^2 (\nabla x_+)^2, \tag{35}$$

with $f_{\rm ex}^\xi = -2.8$, $h^\xi = 2.8$, $f_\nabla^\xi = 2.2$.

All the above values of the parameters were found in Ref. [9] by fitting the masses and charge radii of approximately a hundred spherical nuclei, from calcium isotopes to lead isotopes. In this work, we use this same parameter set for deformed nuclei.

In our current implementation of the Fayans functional in the computer code HFBTHO, for technical reasons we made two small simplifications to the original FaNDF^0 EDF . Firstly, we used the approximation $\rho_{\rm ch} = \rho_{\rm p}$ for the direct Coulomb term. Secondly, we put $f^{\xi}_{\nabla} = 0$ in (35) making the anomalous EDF closer to that used in [10]. Therefore, below we use the above parameters for the normal part of the EDF only. As regards the anomalous EDF, the parameters will be found anew and will be given in the corresponding places. As long as we are dealing with the zero-range pairing force, the strength parameters depend on the cutoff energy $E_{\rm cut}$ in the pairing problem, being also smoothly A dependent [10]. In practice, this means that we take $f^{\xi} = -0.440$ for U and $f^{\xi} = -0.448$ for Pb isotopes.

4. Results

4.1. The uranium chain

We have chosen uranium isotopes for the first application of the FaNDF^0 EDF to deformed nuclei, since most of them have a well established stable deformation. There have been numerous Skyrme EDF studies concerning the deformation landscape of actinide nuclei; see e.g. [56, 57, 58, 59], to list but a few recent studies.

In this work, due to the axial computer code employed, we limit ourselves to the quadrupole deformation β_2 only, with reflection symmetry assumed. We have mainly focused on the ground state characteristics which are, unlike the fission barriers, within the reach of the current axial framework. Indeed, the ground states of U isotopes are expected to be axially deformed. Triaxial deformation, which usually appears at the top of the fission barriers, is neglected in the present study. Also, the role of octupole degrees of freedom becomes important around the second fission barrier in the case of asymmetric fission. For the ground states of uranium isotopes, we present a systematic comparison of our results with those obtained with two versions of Skyrme HFB functionals: HFB-17 and HFB-27 [18].

For the uranium chain, we found that our results converged when the number of oscillator shells was equal to $N_{\rm sh} = 25$, i.e. the change of this number to $N_{\rm sh} = 30$ practically does not influence the results. As regards the pairing force, the set of [9] with $f^{\xi}_{\rm ex} = -h^{\xi}$ corresponds to the 'surface' pairing with a strong attraction at the surface and very small value of f^{ξ} inside a nucleus. Such a model of pairing is typical for all versions of the Fayans functional [10, 25]. Here we have found that the deformation energy for surface pairing is very close to that for the 'volume' pairing model (corresponding to $h^{\xi} = 0$), provided the deformation parameter β_2 is less than 0.3–0.5. To stress the effect of the specific density dependence of the normal part of the Fayans EDF, we use as a rule the simplest one-parameter volume pairing. The cutoff energy $E_{\rm cut} = 60$ MeV is

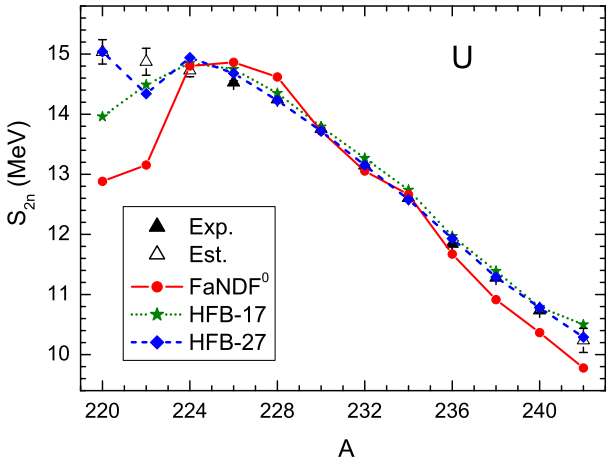

Figure 1. Two-neutron separation energies S_{2n} for even U isotopes. Predictions from the FaNDF^0 functional are compared with those from two Skyrme EDFs: HFB-17 and HFB-27. Empty triangles show the estimated values [68].

chosen, with the corresponding value $f^{\xi} = -0.440$ fitted to the double mass differences for the uranium isotopes.

In figure 1, two-neutron separation energies

$$S_{2n}(N,Z) = B(N,Z) - B(N-2,Z), \tag{36}$$

are shown for uranium isotopes. Comparison is made with experimental data [68] and predictions from the HFB-17 and HFB-27 EDFs. Taking into account that the parameters of the FaNDF^0 functional were fitted only for spherical nuclei not heavier than that of lead, the description of S_{2n} values for uranium isotopes looks rather reasonable. The deviation of 0.5 MeV from the experimental S_{2n} values for heavy U isotopes is explained mainly by two features. The first feature is the use of a simple volume pairing interaction. The second feature is absence of the effective tensor term in the FaNDF^0 EDF. Indeed, as was shown in [52], the tensor term is especially important in uranium and transuranium region as, in the spherical case, high j levels dominate in vicinity of the Fermi level for these nuclei. As a result, the spin-orbit density, which comes to the EDF together with the tensor force, is typically large in these nuclei, changing significantly along the isotopic chain. Accounting for these effects, with the tensor force, represents the essential difference between the DF3a and DF3 EDFs.

In figures 2 and 3, a comparison is presented to the same Skyrme functionals for the deformation energy:

$$E_{\rm def}(\beta_2) = B(\beta_2) - B(\beta_2 = 0), \tag{37}$$

and the deformation parameter itself. Unfortunately, both of these quantities have no direct experimental equivalent. We see that our calculations with the FaNDF^0 functional agree reasonably with both of the Skyrme EDF predictions.

To examine the applicability of the FaNDF^0 functional for the description of large deformations, we have calculated the deformation energy curve for the ^{238}U nucleus

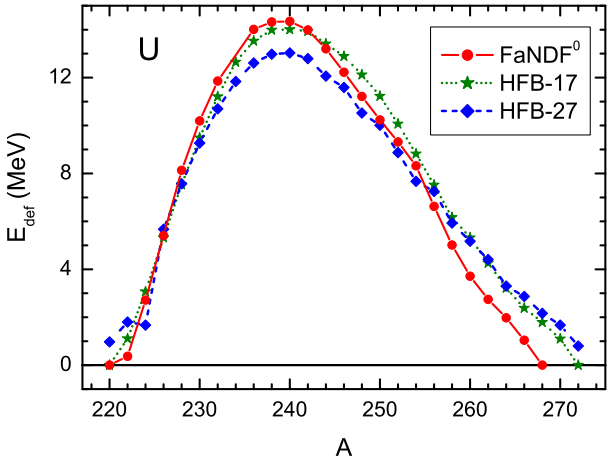

Figure 2. Deformation energy $E_{\rm def}$ for even U isotopes. Predictions from the FaNDF^0 functional are compared with those from two Skyrme EDFs: HFB-17 and HFB-27.

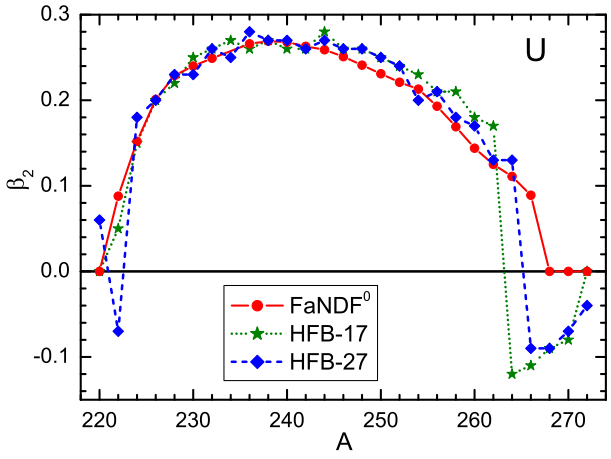

Figure 3. Quadrupole deformation parameter for even U isotopes. Predictions from the FaNDF^0 functional are compared with those from two Skyrme EDFs: HFB-17 and HFB-27.

up to the second fission barrier, shown in figure 4. The calculation scheme remains the same as in the above consideration of the ground states, with a one exception: we have replaced the more simpilied volume pairing interaction with a surface pairing, with parameter values $f^\xi = -1.433$, $h^\xi = 1.375$. This kind of pairing force has been found to be more realistic [9, 10, 25]; see also the *ab initio* consideration of the pairing force in [60]. The difference between the surface and volume pairings becomes important for high deformations, as the role of the surface is strengthened in this case. For example, the second barrier in figure 4 will be 2 MeV higher if we take the volume pairing. For comparison, we also show the results obtained with SLy6 [61], SkM* [62], UNEDF1 [58], and SLy4 [61] Skyrme EDFs. All calculations were carried out within the same calculation scheme as for the FaNDF^0 functional, i.e. with account taken of just the quadrupole deformation, without triaxiality or octupole degrees of freedom.

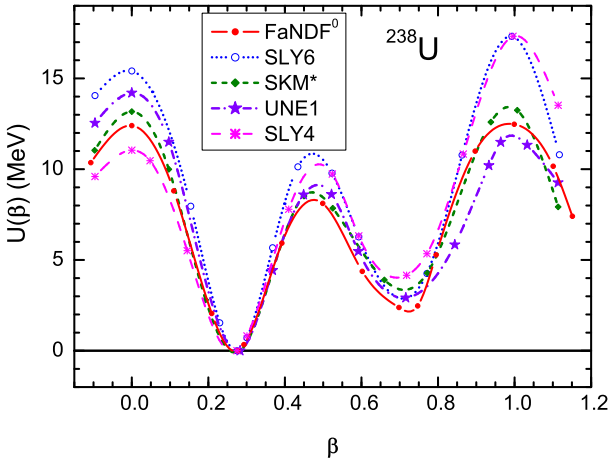

Figure 4. The deformation energy curve for ^{238}U. Predictions from the FaNDF^0 functional are compared with those from four Skyrme EDFs. UNE1 label refers to the UNEDF1 EDF.

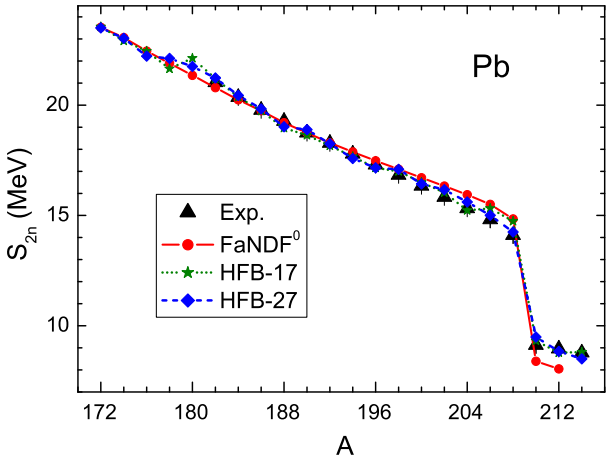

Figure 5. Two-neutron separation energies S_{2n} for even Pb isotopes. Predictions from the FaNDF^0 functional are compared with those from two Skyrme EDFs: HFB-17 and HFB-27.

On neglecting these degrees of freedom, the calculated inner fission barries are typically raised by a few MeV and the outer fission barries, in asymmetric fission, by substantially more; see e.g. [63]. Therefore, it is not meaningful to compare numerical values of the barriers in figure 4 with experimental values directly. However, it is worth noting that the FaNDF^0 curve is rather close to the SkM* and UNEDF1 ones which both, particularly the UNEDF1 one, after the inclusion of triaxial and octupole degrees of freedom, describe uranium barriers reasonably well [58]. On the basis of the results obtained for the uranium isotopes, it seems reasonable to apply this functional for the analysis of the deformation characteristics of other isotopic chains.

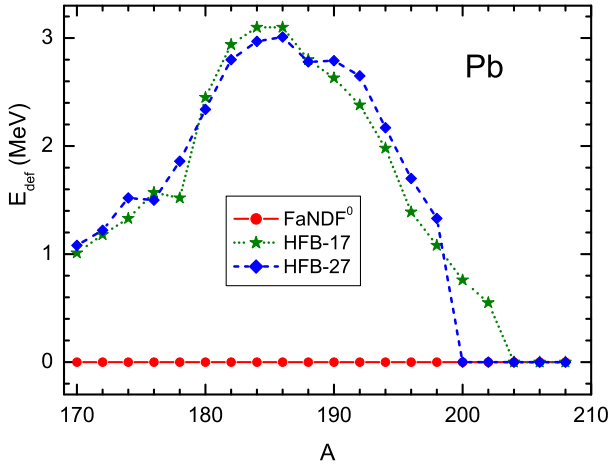

Figure 6. Deformation energy $E_{\rm def}$ for even Pb isotopes. Predictions from the FaNDF^0 functional are compared with those from two Skyrme EDFs: HFB-17 and HFB-27.

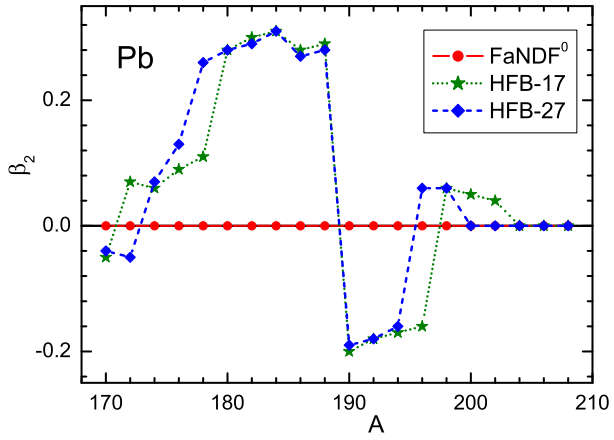

Figure 7. Quadrupole deformation parameter for even Pb isotopes. Predictions from the FaNDF^0 functional are compared with those from two Skyrme EDFs: HFB-17 and HFB-27.

4.2. The lead chain

Our interest to the lead chain is motivated by the observation that HFB-27 and other functionals of this family predict [18] rather strong deformations, $|\beta_2| \simeq 0.2$–0.3, for light $^{180-192}$Pb isotopes. Also, many other Skyrme EDFs seem to predict, at the mean-field level, the appearance of deformation in the region of light Pb isotopes; see e.g. [64, 65]. In our opinion, this does not correspond to the trend of the empirical data on charge radii [20] or magnetic moments [21, 22]. Indeed, charge radii produced by the HFB-27 EDF [18] describe the data for heavy Pb isotopes perfectly well but disagree significantly for those lighter than ^{192}Pb. Analysis of [66] within the generator coordinate method with the use of the Gogny force D1S and of [67] with the SLy6 EDF confirmed the spherical form for these neutron-deficient Pb isotopes. Although in both studies the

angular momentum projection technique was used, the simplest mean-field calculation also did not predict so large deformations as in [18]. Thus predictions of different Skyrme functionals for the light Pb isotopes are essentially different. Therefore it is of interest to look at how the FaNDF^0 functional behaves for these nuclei and compare our predictions with those of various Skyrme EDFs.

In the analysis of the lead isotopes, we use the same calculation scheme as for the uranium chain, i.e. $N_{\rm sh} = 25$ and $E_{\rm cut} = 60$ MeV are chosen, and the corresponding value $f^{\xi} = -0.448$ is a bit different in order to provide a better description of the S_n and S_{2n} values on average. We again begin with the two-neutron separation energies S_{2n}, shown in figure 5. On average, the agreement with the data obtained with FaNDF^0 is only a little less good compared to the case for the HFB-17 and HFB-27 functionals. The agreement of the S_{2n} values with the experiment for the heaviest Pb isotopes will be better if we use the surface pairing, which is more realistic as is discussed above. However, a new readjustment of FaNDF^0 parameters with tensor terms added is necessary for competing with HFB EDFs in the accuracy of reproducing the binding energies.

As regards the deformation characteristics, there is a notable difference between predictions from the Fayans FaNDF^0 EDF and those from the two Skyrme functionals under consideration. Namely, calculations with the Fayans functional result to a spherical mean-field ground state for all of the lead isotopes. At the same time, the HFB-17 and HFB-27 functionals both predict a stable deformation in the ground states for many light Pb isotopes, as shown in figure 7. For the HFB-27 functional, deformation appears for isotopes with $A = 170$–198, and for the HFB-17 functional, for all isotopes with $A < 204$. For both the functionals, the deformation changes sign from positive for ^{188}Pb to negative for ^{190}Pb, and the deformation is strong for isotopes with $A = 180$–192; $\beta_2 \simeq 0.3$ for $A = 180$–188 and $\beta_2 \simeq -0.2$ for $A = 190$–194 in the case of the HFB-27 functional and for $A = 190$–196 in the case of the HFB-17 one. Thus, the value of the deformation parameter within this mass-region is approximately of the same order of magnitude as for the uranium isotopes. The deformation energy is less, $E_{\rm def} \simeq 3$ MeV, and also not negligible, as shown in figure 6. To summarize, the predictions of both of these HFB functionals do not follow experimental data trends on charge radii and magnetic moments, as was discussed above. In addition, they disagree with the predictions of [67] for the SLy6 EDF.

To investigate the problem in more detail, we have calculated the deformation energy curves $U(\beta)$ for several light Pb isotopes with the FaNDF^0 functional and the same Skyrme EDFs as for the case of ^{238}U. The results are shown in figure 8. We begin comparison with the doubly magic ^{208}Pb, shown in panel (a). All four curves behave in a similar way, which corresponds to the very rigid nature of this nucleus. The positions of the first barrier and the second minimum are almost the same for all of the EDFs. For the small deformation region, FaNDF^0 and UNEDF1 curves show very similar behavior. The SkM* deformation energy curve seems to be the one closest to FaNDF^0, and only SLy6 deformation energy is notably higher, by 4–5 MeV at $\beta_2 = 0.3$–0.6.

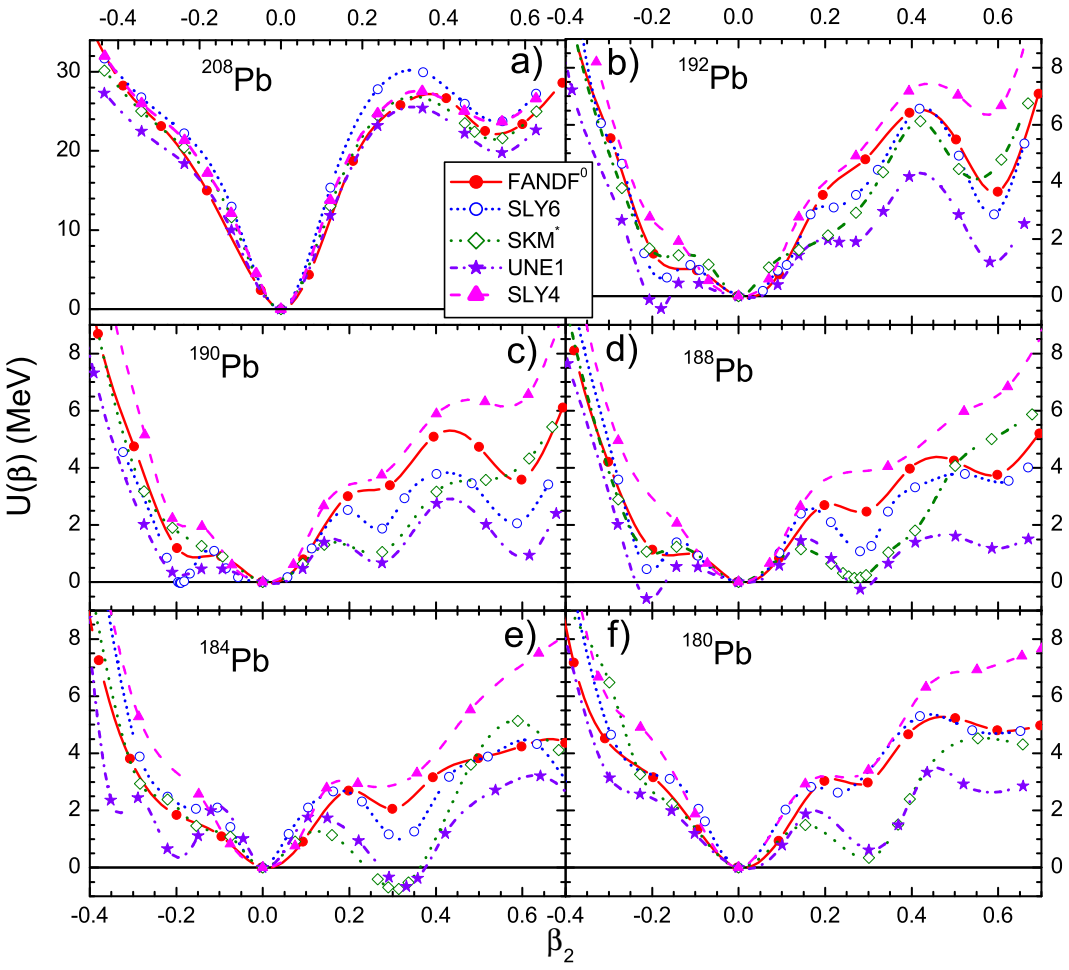

Figure 8. Deformation energy curves $U(\beta)$ for Pb isotopes as a function of the deformation β for FaNDF^0 and various Skyrme EDFs. Shown are the results for ^{208}Pb (a), ^{192}Pb (b), ^{190}Pb (c), ^{188}Pb (d), ^{184}Pb (e), and ^{180}Pb (f).

Next, we investigate the light isotopes, which are of our main interest in the present work. For ^{192}Pb nucleus, shown in figure 8, panel (b), the FaNDF^0 deformation energy follows the SLy6 and SkM* ones rather closely, being rather rigid at the minimum of $\beta = 0$. Only the UNEDF1 curve behaves softer predicting an oblate, $\beta_2 \simeq -0.2$, ground state. The SLy4 EDF is the most rigid. The latter is true also for the ^{190}Pb nucleus, shown in panel (c). The behavior of the FaNDF^0 curve here is also rather rigid, but softer compared to ^{192}Pb. It has a shallow minimum, roughly 1 MeV above the ground state energy, at $\beta_2 \simeq$ -(0.1–0.2). According to the remaining three Skyrme EDF predictions, this nucleus is much softer. All of the corresponding Skyrme functions possess clearly distinguishable minima at the prolate deformation, $\beta_2 \simeq 0.3$. The corresponding excitation energies are about 2 MeV for SLy6, 1 MeV for SkM* and only 0.5 MeV for the UNEDF1 EDF. For oblate deformations, UNEDF1 and SLy6 EDFs lead to very low minima at $\beta_2 \simeq -0.2$, the latter being a little lower than the spherical one. As mentioned, these predictions are based on the single-reference mean-field level.

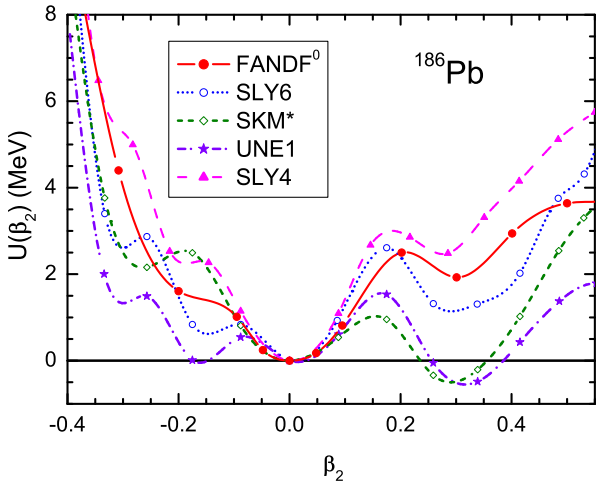

Figure 9. Deformation energy curves $U(\beta)$ for the ^{186}Pb nucleus.

Corrections to this scheme leads to a restoration of the spherical form for this nucleus [67].

For the ^{188}Pb nucleus, shown in panel (d) of figure 8, the situation is similar, but now both of the deformed UNEDF1 minima are lower compared to the spherical one. The SkM* minimum is higher than the spherical one, but only a bit. The FaNDF^0 curve is qualitatively similar to the SLy6 one, but a little more rigid. For the ^{184}Pb, shown in panel (e), SkM* and UNEDF1 EDFs predict a prolate ground state at $\beta_2 \simeq 0.3$. Finally, the ^{180}Pb nucleus, shown in panel (f), becomes much more rigid than the nuclei considered above.

In figure 9, we show separately the deformation energy curves for the ^{186}Pb nucleus possessing, in addition to the ground state, two exited low-lying 0^+ states, an oblate and a prolate one, with excitation energy of about 1 MeV. As shown in [66] and [67], it is necessary to go beyond the plain mean field theory to describe their characteristics correctly. Here, the mean field picture gives a rough estimate which of the EDFs has the better chance of providing a successful description of these states in calculations beyond the mean field level. In [67], SLy6 was found to reproduce these state successfully. Here, the FaNDF^0 curve is again qualitatively similar to SLy6, but both minima are approximately 1 MeV higher.

To conclude this section, we note that predictions from different Skyrme EDFs for light lead isotopes are found to be quite different. The SLy4 EDF is the most rigid of all functionals under consideration, including FaNDF^0. On the other hand, FaNDF^0 predicts spherical form for all the lead isotopes. Probably, this could be explained with the influence of the denominator of equation (25), which provides some feedback preventing the deformation of the light Pb isotopes. At the same time, FaNDF^0 predictions are rather close to SLy6 ones, with exception of those for the ^{190}Pb nucleus.

5. Conclusion

This work presents the first application of the Fayans functional FaNDF^0 [9] to deformed nuclei. The Fayans functional makes an interesting alternative to the Skyrme EDF with some promising properties, as shown in the current work. A systematic comparison for the mean-field deformations and deformation energies was made against two modern Skyrme EDFs: HFB-17 and HFB-27. Results were calculated for the uranium and lead isotopic chains. In the uranium case, our results are qualitatively close to both the HFB-17 and HFB-27 functional results.

To check the applicability of the Fayans functional for description of large deformation, we calculated the deformation energy curve for ^{238}U nucleus with FaNDF^0 and four different Skyrme EDFs. Our result turned out to be rather close to the SkM* and UNEDF1 ones. These two Skyrme parameterizations, in particularly UNEDF1, after inclusion of the octupole deformation and triaxiality, reproduce values of the experimental first and second barriers in this nucleus sufficiently well [58]. Here, in the present work, we limit ourselves to just the quadrupole deformation only due to limitations of the used computer code. For the ^{238}U, the results obtained in axial framework for FaNDF^0 are rather close to those of most successful Skyrme EDFs. Nevertheless, with the current calculation scheme, it is too early to draw any concrete conclusions about the fission properties of FaNDF^0.

For the lead isotopes, however, there was some notable differences between FaNDF^0 and Skyrme EDFs. Here, both of the HFB functionals predict strong deformation of the light isotopes: $A = 178$–196 for the functional HFB-17 and $A = 178$–194 for HFB-27. This does not agree to experimental data on the charge radii [20] and magnetic moments [21, 22]. On the contrary, the Fayans functional predicts spherical mean-field solution for all Pb isotopes, in agreement with experimental trend. To examine these differences, we calculated deformation energy curves for several light lead isotopes. Again the FaNDF^0 results are compared to those obtained with four Skyrme EDFs. The predictions from the different Skyrme EDFs are quite different, the FaNDF^0 ones being rather close to those from the SLy6 EDF.

Thus, the FaNDF^0 functional, with the parameters adjusted to spherical nuclei, seems to describe rather well the ground state deformation properties of the two isotopic chains studied in the present work. This feature may be linked to a peculiar density dependence of the Fayans functional, resulting from the energy dependence effects of the self-consistent TFFS [19] which are hidden in the formulation in terms of the EDF. A systematic analysis of deformed nuclei with the Fayans functional would be necessary to estimate its possible benefits across larger portions of the nuclear chart. Also, to address the fission properties of the FaNDF^0, fully triaxial calculations are required.

6. Acknowledgments

We are grateful to Michael Bender for useful comments. The work was partly supported by the Grant NSh-932.2014.2 of the Russian Ministry for Science and Education, by the RFBR Grants 12-02-00955-a, 13-02-00085-a, 13-02-12106_ofi-m, 14-02-00107-a, 14-22-03040_ofi-m, the Grant by IN2P3-RFBR under Agreement No. 110291054, and Swiss National Scientific Foundation Grant No. IZ73Z0_152485 SCOPES. This work was also supported (M.K.) by the Academy of Finland under the Centre of Excellence Programme 2012–2017 (Nuclear and Accelerator Based Physics Programme at JYFL) and the FIDIPRO programme; and by the European Unions Seventh Framework Programme ENSAR (THEXO) under Grant No. 262010.

References

[1] Vautherin D and Brink D M 1972 *Phys. Rev.* C **5** 626
[2] Dechargé J and Gogny D 1980 *Phys. Rev.* C **21** 1568
[3] Ring P 1996 *Prog. Part. Nucl. Phys.* **37** 193
[4] Ring P and Schuck P 1980 *The Nuclear Many-Body Problem* (Springer-Verlag, New York).
[5] M. Bender, Heenen P-H and Reinhard P-G 2003 *Rev. Mod. Phys.* **75** 121 .
[6] Smirnov A V, Tolokonnikov S V and Fayans S A 1988 *Sov. J. Nucl.* Phys. **48** 995
[7] Horen D J, Satchler G R, Fayans S A and Trykov E L 1996 *Nucl. Phys.* A **600** 193
[8] Borzov I N, Fayans S A, Kromer E, Zawischa D 1996 *Z. Phys.* A **355** 117
[9] Fayans S A 1998 *JETP Letters* **68** 169
[10] Fayans S A, Tolokonnikov S V, Trykov E L and Zawischa D 2000 *Nucl. Phys.* A **676** 49
[11] Dobaczewski J, Carlsson B G and Kortelainen M 2010 *J. Phys.* G: Nucl. Part. Phys. **37** 075106
[12] Gebremariam B, Duguet T and Bogner S K 2010 *Phys. Rev.* C **82** 014305
[13] Kaiser N, Weise W 2010 *Nucl. Phys.* A **836** 256
[14] Carlsson B G and Dobaczewski J 2010 *Phys. Rev. Lett.* **105** 122501
[15] Gebremariam B, Bogner S K and Duguet T 2011 *Nucl. Phys.* A **851** 17
[16] Stoitsov M, Kortelainen M, Bogner S K, Duguet T, Furnstahl R J, Gebremariam B and Schunck N. 2010 *Phys. Rev.* C **82** 054307
[17] Goriely S, Chamel N. and Pearson J M 2009 *Phys. Rev. Lett.* **102** 152503
[18] Goriely S http://www-astro.ulb.ac.be/bruslib
[19] Khodel V A and Saperstein E E 1982 *Phys. Rep.* **92** 183
[20] Saperstein E E and Tolokonnikov S V 2011 *Phys. At. Nucl.* **74** 1277
[21] Borzov I N, Saperstein E E and Tolokonnikov S V 2008 *Phys. At. Nucl.* **71**, 469
[22] Borzov I N, Saperstein E E, Tolokonnikov S V, Neyens G and Severijns N 2010 *Eur. Phys. J.* A **45** 159
[23] Tolokonnikov S V, Kamerdzhiev S, Krewald S, Saperstein E E and Voitenkov D 2012 *Eur. Phys. J.* A **48** 70
[24] Kamerdzhiev S, Krewald S, Tolokonnikov S V, Saperstein E E and Voitenkov D 2012 *Eur. Phys. J.* Web of Conferences **38** 10002
[25] Tolokonnikov S V, Kamerdzhiev S, Voytenkov D, Krewald S and Saperstein E E 2011 *Phys. Rev.* C **84** 064324
[26] Tolokonnikov S V, Kamerdzhiev S, Krewald S, Saperstein E E and Voitenkov D 2012 *Eur. Phys. J.* Web of Conferences **38** 04002
[27] Borzov I N 2006 *Nucl. Phys.* A **777** 645
[28] Gnezdilov N V, Borzov I N, Saperstein E E, and Tolokonnikov S V 2014 *Phys. Rev.* C **89** 034304
[29] Baldo M, Maieron C, Schuck P and Viñas X 2004 *Nucl. Phys.* A **736** 241
[30] Baldo M, Schuck P and Viñas X 2008 *Phys. Lett.* B **663** 390
[31] Robledo L M, Baldo M, Schuck P and Viñas X 2008 *Phys. Rev.* C **77** 051301(R)
[32] Robledo L M, Baldo M, Schuck P and Viñas X 2010 *Phys. Rev.* C **81** 034315
[33] Baldo M, Robledo L M, Schuck P and Viñas X 2010 *J. Phys. G: Nucl. Part. Phys.* **37** 064015
[34] Robledo L M, Baldo M, Schuck P and Viñas X 2011 *Journal of Physics: Conference Series* **321** 012015
[35] Baldo M, Robledo L M, Schuck P and Viñas X 2013 *Phys. Rev.* C **87** 064305
[36] Giuliani Samuel A and Robledo Luis M 2013 *Phys. Rev.* C **88** 054325
[37] Giuliani Samuel A, Robledo Luis M and Rodírguez-Guzmán R 2014 *Phys. Rev.* C **90** 054311
[38] Friedman B and Pandharipande V R 1988 *Nucl. Phys.* **48** 995
[39] Stoitsov M V, Schunck N, Kortelainen M, Michel N, Nam H, Olsen E, Sarich J and Wild S 2013 *Comp. Phys. Comm.* **184** 1592
[40] Migdal A B 1967 *Theory of finite Fermi systems and applications to atomic nuclei* (Nauka, Moscow, 1965; Wiley, New York).

[41] Fayans S A and Khodel V A 1973 *JETP Lett.* **17** 444
[42] Saperstein E E, Tolokonnikov S V 1998 *JETP Lett.* **68** 553
[43] Kohn W and Sham L J 1965 *Phys. Rev.* **140** A1133
[44] Oliveira L N, Gross E K U and Kohn W 1988 *Phys. Rev. Lett.* **60** 2430
[45] Belyaev S T, Smirnov A V, Tolokonnikov S V, Fayans S A 1987 *Sov. J. Nucl. Phys.* **45** 783
[46] Dobaczewski J, Flocard H and Treiner J 1984 *Nucl. Phys.* A 422 103
[47] Hohenberg P and Kohn W 1964 *Phys. Rev.* **136** B864
[48] Dobaczewski J, Stoitsov M V, Nazarewicz W and Reinhard P-G 2007 *Phys. Rev.* C **76** 054315
[49] Lacroix D, Duguet T and Bender M 2009 *Phys. Rev.* C **79** 044318
[50] Bender M, Duguet T and Lacroix D 2009 *Phys. Rev.* C **79** 044319
[51] Satuła W, Dobaczewski J, Nazarewicz W and Rafalski M 2011 *Int. J. Mod. Phys.* **E20** 244
[52] Tolokonnikov S V and Saperstein E E 2010 *Phys. At. Nucl.* **73** 1684
[53] Dutra M, Lourenceo O, Sá Martins J S, Delfino A, Stone J R and Stevenson P D 2012 *Phys. Rev.* C **85** 035201
[54] Nolen J A, Schiffer J P 1969 *Annu. Rev. Nucl. Sci.* **19**
[55] Brown B A 1998 *Phys. Rev.* C **58** 220
[56] Goriely S, Hilaire S, Koning A, Sin M and Capote R 2009 *Phys. Rev.* C **79** 024612
[57] Staszczak A, Baran A, Dobaczewski J, Nazarewicz W 2009 *Phys. Rev.* C **80** 014309
[58] Kortelainen M, McDonnell J, Nazarewicz W, Reinhard P-G, Sarich J, Schunck N, Stoitsov M V and Wild S M 2012 *Phys. Rev.* C **85** 024304
[59] McDonnell J D, Nazarewicz W and Sheikh J A 2013 *Phys. Rev.* C **87** 054327
[60] Pankratov S S, Baldo M, Lombardo U, Saperstein E E and Zverev M V 2011 *Phys. Rev.* C **84** 014321
[61] Chabanat E, Bonche P, Haensel P, Meyer J and Schaeffer R 1998 *Nucl. Phys.* A **635** 231
[62] Bartel J, Quentin P, Brack M, Guet C and Håkansson H B 1982 *Nucl. Phys.* A **386** 79
[63] Bürvenich T, Bender M, Maruhn J and Reinhard P.-G 2004 *Phys. Rev.* C **69** 014307
[64] Stoitsov M V, Dobaczewski J, Nazarewicz W, Pittel S and Dean D J 2003 *Phys. Rev.* C **68** 054312
[65] Erler J, Birge N, Kortelainen M, Nazarewicz W, Olsen E, Perhac A M and Stoitsov M 2012 *Nature* **486** 509
[66] Rodrguez-Guzmán R R, Egido J L and Robledo L M 2004 *Phys. Rev.* C **69** 054319
[67] Bender M, Bonche P, Duguet T and Heenen P-H 2004 *Phys. Rev.* C **69** 064303
[68] Audi G, Wapstra A H and Thibault C 2003 *Nucl. Phys.* A **729** 337